AMERICAN SOCIETY of
GENE & CELL
THERAPY

Ultrasound Assisted Exosomal Delivery of Tissue Responsive mRNA for Enhanced Efficacy and Minimized Off-Target Effects

Wenqi Sun,[1,2,3] Changyang Xing,[1,3] Lianbi Zhao,[1,2,3] Ping Zhao,[1] Guodong Yang,[2] and Lijun Yuan[1]

[1]Department of Ultrasound Diagnostics, Tangdu Hospital, Fourth Military Medical University, Xi'an 710038, People's Republic of China; [2]The State Laboratory of Cancer Biology, Department of Biochemistry and Molecular Biology, Fourth Military Medical University, Xi'an 710032, People's Republic of China

Exosome-mediated nucleic acids delivery has been emerging as a promising strategy for gene therapy. However, the intrinsic off-target effects due to non-specific uptake of exosomes by other tissues remain the big hurdle for clinical application. In this study, we aimed to enhance the efficacy and minimize the off-target effects by simultaneously encapsulating engineered mRNA translationally activated by tissue-specific microRNA (miRNA) and increasing targeted delivery efficiency via ultrasound-targeted microbubble destruction (UTMD). Briefly, the upstream of interest transcript was engineered to harbor an internal ribosome entry site (IRES) modified with two miRNA recognition sites. *In vitro* reporter experiments revealed that the engineered mRNA could be encapsulated into exosomes and can be translationally activated by corresponding miRNAs in the recipient cells. By a proof-of-principle *in vivo* experiment, we encapsulated miR-148a (an adipose relatively specific miRNA)-responsive PGC1α mRNA into exosomes and delivered the exosomes into the adipose tissue with the aid of UTMD. Efficient PGC1α translation was activated in the adipose tissue, together with obvious browning induction. Moreover, there was much lower off-target translation of PGC1 α in lungs and other tissues. Taken together, our study establishes a novel adipose-specific exosome delivery strategy to enhance efficacy and minimize off-target effects simultaneously.

INTRODUCTION

Exosomes, which are cell-derived vesicles 30–150 nm in diameter, are emerging as a promising drug carrier for gene therapy.[1] Briefly, the nucleic acids of interest could be either loaded by electroporation in the isolated exosomes or encapsulated during exosome biogenesis in the donor cells.[2,3] Theoretically, both the non-coding RNAs and mRNAs could be loaded into the exosomes for gene therapy, although most of the studies focused on the non-coding RNAs.

Compared to chemically synthesized nanoparticles, exosomes have been reported to be resistant to clearance by the reticuloendothelial system and be able to cross multiple biological barriers.[3,4] However, there are still abundant exosomes delivered that are found in tissues other than the targeted organ, even when the targeting moieties are included.

Therapeutically minimizing the non-specific off-target effects is of great importance for future clinical application.

Besides targeted delivery, tissue-specific expression of the delivered genes holds promise for minimizing the off-target effects at another layer. Previously, tissue-specific promoters have been commonly used for conditional gene expression, although the strategy controls gene expression at the transcriptional level and only works when DNA is delivered.[5] Tissue-specific control of gene expression at the translational level would allow the delivered RNA to only work in the targeted tissue. Formerly, liver-specific miRNA-122 (miR-122) was found to recognize two conserved sites at the IRES region of the 5′ end of the hepatitis C virus (HCV) genome, and thus regulates the stability, translation, and replication of the viral RNA.[6] The data suggest that mRNA could be modified to be regulated by tissue-specific miRNAs, and thus its expression could be controlled in a tissue-specific manner.

In this study, we aimed to minimize the off-target effects by simultaneously encapsulating engineered mRNA translationally activated by tissue-specific miRNA and by increasing targeted delivery efficiency via ultrasound-targeted microbubble destruction (UTMD). By a proof-of-principle experiment, we encapsulated miR-148a (an adipose relatively specific miRNA)-responsive PGC1α mRNA into exosomes and delivered the exosomes into the visceral adipose tissue with the aid of UTMD. Efficient PGC1α translation was activated in the adipose tissue, together with obvious browning induction. Moreover, there was much lower off-target translation of PGC1α in the lungs. Taken together, our study establishes a novel exosome delivery strategy to minimize off-target effects.
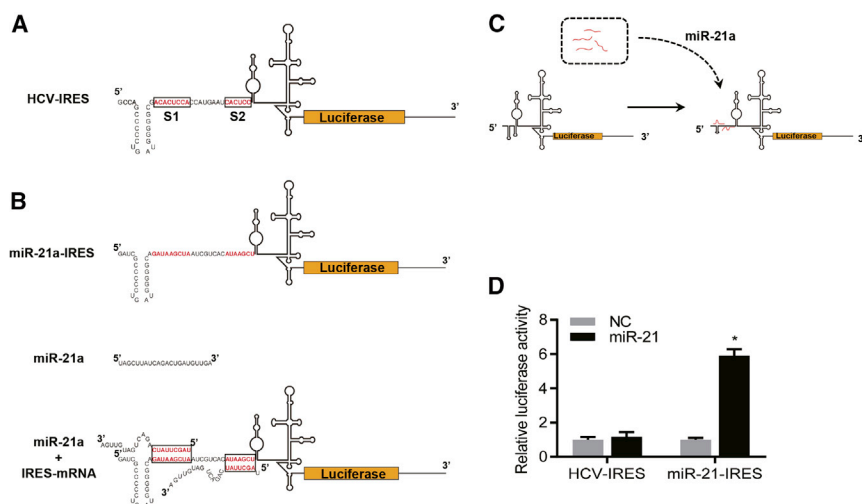
Figure 1. Construction of miRNA-Responsive mRNA Translation System

(A) Schematic cartoon of the reporter gene whose translation is driven by the HCV IRES. (B) The native miR-122 recognition sites S1 and S2 of the HCV IRES were mutated to the sequence recognized by miR-21a. (C) Theoretical conformational change of the IRES structure in the presence of miR-21a. (D) Relative luciferase activity of the reporter gene. Data are expressed as mean ± SEM. *p < 0.05 versus NC.

RESULTS

Construction of miRNA-Responsive mRNA Translation System

RNA delivery holds great promise for gene therapy; however, specifically activating mRNA translation in a cell type-specific manner remains a challenge. Previous studies have found that miRNA expression displays a cell type-specific pattern.[7] Meanwhile, miRNAs have been found to activate IRES-mediated translation during virus infection.[8] To further confirm whether miRNAs could activate IRES-mediated translation in a sequence-dependent manner as a universal rule, a luciferase based reporter assay was included. An IRES sequence was engineered upstream of the luciferase coding sequence (CDS) in the reporter plasmid by molecular cloning (Figure 1A). For miRNA-specific activation, the sequences of sites 1 and 2 (denoted as S1 and S2 hereafter) corresponding to the HCV-IRES region in the reporter plasmid were mutated to be recognition sites for miRNAs of interest, such as miR-21a (Figure 1B). The resultant miR-21a-responsive IRES-Luc reporter was denoted as miR-21a-IRES-Luc. Theoretically, miR-21a binding to the S1 and S2 regions would induce a conformational change of the IRES, and thus affect the RNA stability and translation efficiency (Figures 1B and 1C). As expected, co-transfection of miR-21a and miR-21a-IRES-Luc significantly increased the relative luciferase activity, whereas the negative control (NC) miRNA mimics had minimal effects (Figure 1D). Similarly, the S1 and S2 sequences were mutated to miR-211 and miR-148a recognition sites, and co-transfection of corresponding miRNAs significantly increased the luciferase activity (Figures S1A–S2C and S2A–S2C). All of the above data suggest that miRNA could activate IRES-mediated translation in a sequence-specific manner.

Next, we asked whether the IRES-Luc translation system could respond differently in cell types with differential miRNA expression. B16 cells had significantly higher expression of miR-21a compared with HEK293T cells (Figure S3A). Accordingly, the miR-21a-IRES-Luc reporter had a much higher luciferase activity in the B16 cells, compared with that in the HEK293T cells (Figure S3B).

Encapsulation of the miRNA-Responsive mRNA Translation System into Exosomes

The above data suggest that delivery of miRNA-IRES-mRNA might be responsive in a cell type-specific manner in vivo. To deliver the miRNA-IRES-mRNA in vivo, we focused on the exosome system. Exosome packaging HEK293T cells were transfected with the IRES-Luc reporter plasmid before exosome isolation (Figure 2A). The isolated exosomes had typical exosome morphology, size distribution, and protein markers (Figures 2B–2D). As expected, the isolated exosomes had robust IRES-Luc mRNA encapsulation (Figure 2E). Moreover, absolute quantification PCR analysis revealed that there were about 50–70 mRNA copies encapsulated per 100 exosomes.

Next, we asked whether the exosome-encapsulated IRES-Luc mRNA was functional and responsive to the corresponding miRNA. Exosomes loaded with miR-21a-IRES-Luc or control Cap-Luc (without IRES) were isolated and separately added into HEK293T or B16 cells, and exosomes loaded with Renilla mRNA (derived from the pRL-TK-transfected cells) acted as the internal control. After exosomes were added, the miR-21a mimics or inhibitors were transfected (Figure 3A). Exosomes loaded with Cap-Luc produced similar luciferase activity in both cells, which was not affected by miR-21a intervention (Figures 3B and 3C). Treatment of exosomes loaded with miR-21a-IRES-Luc produced much lower luciferase activity in HEK293T cells, whereas miR-21a transfection significantly enhanced the luciferase activity (Figure 3B). In contrast, treatment of exosomes loaded with miR-21a-IRES-Luc produced robust luciferase activity in B16 cells, while miR-21a inhibition significantly blocked the luciferase activity (Figure 3C).

To further exclude the possibility that the differences were caused by the encapsulated luciferase protein, the miR-21a-IRES-GFP expression system was included. In the miR-21a-IRES-GFP system, the firefly luciferase open reading frame (ORF) was replaced by the GFP ORF. After isolation of the exosomes from miR-21a-IRES-GFP-transfected HEK293T cells, the exosomes were exposed to light for 12 h to photo-quench the GFP protein (Figure 3D). Then, the exosomes were added to HEK293T cells and detected by confocal laser scanning microscopy (CLSM) right after co-culture or 24-h co-culture (Figure 3D). As expected, the photo-quenched exosomes had no obvious GFP signal right after incubation. However, there was significant GFP
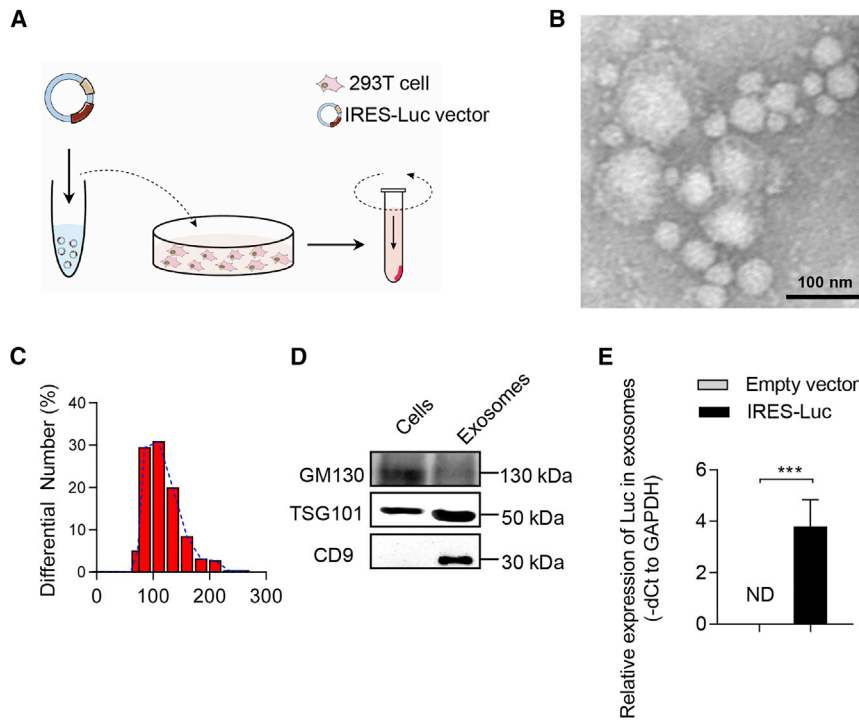
Figure 2. Encapsulation of the miRNA-Responsive mRNA Translation System into Exosomes

(A) Schematic illustration of the exosome biogenesis and isolation procedure. (B) Representative transmission electron microscopy (TEM) image of the isolated exosomes. (C) Size distribution of the isolated exosomes. (D) Western blot analysis of the exosomal inclusive (TSG101, CD9) and exclusive (GM130) markers. Representative images of three different experiments are shown. (E) qPCR analysis of miR-21a-IRES-Luc mRNA in exosomes isolated from control and miR-21a-IRES-Luc plasmid-transfected HEK293T cells. Data are expressed as mean ± SEM of three independent experiments. ***p < 0.001 versus empty vector. ND, not detected.

expression in the B16 cells following 24-h culture (Figure 3E). Consistent with the luciferase data, treatment of the exosomes loaded with miR-21a-IRES-GFP produced no obvious GFP expression in the HEK293T cells (Figures S4A and S4B), while miR-21a transfection significantly activated the GFP expression (Figure S4B). All of the above data indicate that the encapsulated miRNA-IRES-mRNA is functional in the recipient cells when the corresponding miRNA is endogenously abundant.

UTMD Assists Adipose Delivery of Exosomes

In view of the above data, we speculated that delivery of IRES-mRNA responding to tissue-specific miRNA *in vivo* could minimize the off-target effects. Consistent with previous studies, exosomes were preferentially localized in the liver, spleen, and lung (Figure S5A), whereas adipose tissue was intrinsically resistant to exosome delivery (Figures 4A and 4B). To this end, the UTMD technique was used to facilitate the exosome delivery to these refractory tissues.[9] Consistent with our previous findings, delivery of exosomes to the organs, such as the heart, liver, and spleen, was enhanced when they received irradiation (Figure S5A). Similarly, UTMD also significantly increased the delivery of exosomes into the adipose tissue (Figures 4B and 4C). Moreover, the local UTMD in the left side of the omental tissue region had minimal effects on the exosome delivery into liver, spleen, and lung, as well as the intestine beyond the irradiated region, as revealed by *cel*-miR-39 tracking (Figures 4D and 4E). Notably, ultrasound can pierce through tissues, and thus an increase of exosome delivery in the irradiated small intestine was also observed (Figure S5A), suggesting that additional off-target prevention strategies are strongly needed.

Delivery of miR-148a-IRES-PGC1α Minimizes the Off-Target Effects

miR-148a was found to be abundantly expressed in the adipose tissue, and it functions importantly in adipogenesis.[10] qPCR profiling data further confirmed the relatively high specificity of miR-148a in adipose tissue in both chow diet and high fat-diet (HFD) mice (Figures 5A and 5B), suggesting that miR-148a-IRES-mRNA might be translationally active in adipose tissue. Previous studies have found that PGC1α is an essential transcription factor for fat browning.[11] We thus asked whether delivery of miR-148a-responsive IRES-PGC1α could induce fat browning *in vivo* efficiently while having minimal off-target effects. The PGC1α ORF was placed downstream of the miR-148a-IRES, with the clone being denoted as miR-148a-IRES-PGC1α hereafter (Figure 5C). Followed by miR-148a transfection, robust translation of PGC1α was induced in B16 cells transfected with miR-148a-IRES-PGC1α expression plasmid (Figure 5D), to a similar level as the common cap-dependent PGC1α expression system.

To deliver miR-148a-IRES-PGC1α *in vivo*, miR-148a-IRES-PGC1α expression plasmid was transfected into HEK293T cells, and the empty plasmid and routine PGC1α expression plasmid without IRES (namely Cap-PGC1α) served as controls, followed by exosome isolation (Figure 6A). As expected, miR-148a-IRES-PGC1α mRNA was enriched in the exosomes derived from the HEK293T cells transfected with miR-148a-IRES-PGC1α (Figure 6B). Similar PGC1α RNA levels were found in exosomes derived from cells transfected with either miR-148a-IRES-PGC1α or Cap-PGC1α (Figure 6B). In contrast, no PGC1α protein was found in any of the exosomes, which might be explained by the nuclear localization of PGC1α (Figure S6A). In the following experiments, we delivered the exosomes loaded with miR-148a-IRES-PGC1α or Cap-PGC1α into adipose tissue with the aid of UTMD. In the adipose tissue of mice treated with exosomes loaded with miR-148a-IRES-PGC1α or Cap-PGC1α, there was a significant increase of PGC1α protein expression (Figure 6C). With regard to the lung tissue, which had low miR-148a expression (Figures 5A and 5B), PGC1α translation was only induced in mice treated
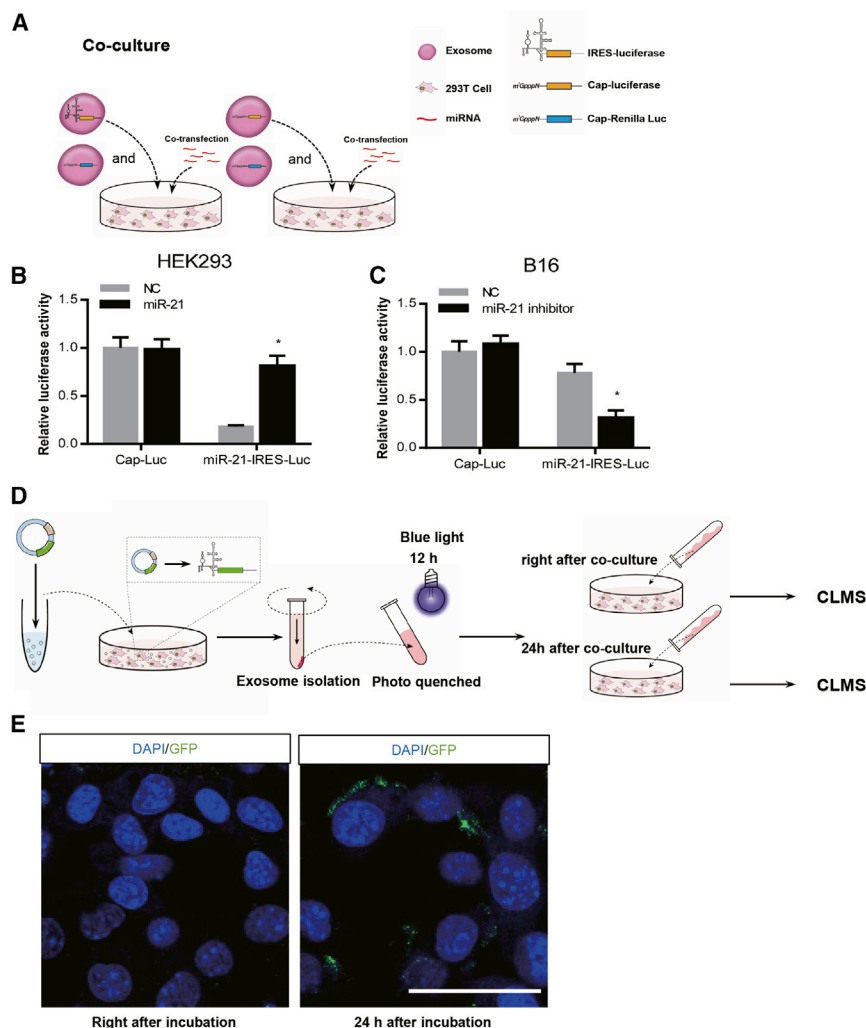
Figure 3. Exosome-Encapsulated miRNA-Responsive mRNA Translation System Is Functional in Recipient Cells

(A) Schematic illustration of the experimental procedure. HEK293T cells were transfected with control Luc expression plasmid (Cap-Luc) or miR-21a-IRES-Luc plasmid, and switched to DMEM medium without FBS for additional culture of 36 h before exosome isolation. The isolated exosomes thus contained Cap-Luc or miR-21a-IRES-Luc, respectively. The pRL-TK-transfected HEK293T cells were used for isolation of Cap-Renilla Luc-containing exosomes. About 50 ng of isolated exosomes (30 ng of exosomes of Cap Luc or miR-21a-IRES-Luc, plus 20 ng of exosomes of Cap-Renilla Luc) was added into HEK293T cells placed in 24-well plates and co-transfected with miR-21a mimics. The luciferase activity was analyzed 24 h after exosome treatment. (B and C) Relative luciferase activity in HEK293T (B) and B16 (C) cells treated as indicated. Data are expressed as mean- ± SEM. *p < 0.05 versus NC. (D) Schematic illustration of the experimental procedure. Luciferase ORF in the miR-21a-IRES-Luc plasmid was replaced with GFP ORF. Additionally, the exosomes from miR-21a-IRES-Luc-transfected HEK293T cells were photo-quenched by exposing the exosomes to blue light for 12 h. Then, the exosomes were added to B16 cells. The GFP expression was analyzed right after exosome addition and 24 h later. (E) Representative images of the GFP expression in B16 cells. Scale bar, 20 μm.

with the Cap-PGC1α exosome group (Figure 6D), suggesting minimized off-target effects of the miR-148a-IRES-PGC1α group in the lung. Similarly, significantly smaller off-target effects were also observed in other organs, such as spleen and kidney (Figure S6B), whereas no obvious reduced off-target effects were observed in liver and heart (Figure S6B), which could be explained by similar miR-148a expression in liver (Figures 5A and 5B) and low delivery efficiency in the heart (Figures 5A and 5B). Since exosomes were intrinsically delivered into liver, spleen, and lung, we thus examined the potential toxic effects in these organs. H&E staining revealed that no obvious inflammation or other damages were observed even in the UTMD-assisted Cap-PGC1α group (Figure S7), further suggesting that the proposed exosome-based strategy should be considered as one of the safest strategies to deliver nucleic acids.

Adipose-Specific PGC1α Expression Promotes Browning in HFD Mice

Next, we asked whether delivery of mIRES-PGC1α produced similar browning effects as delivery of Cap-PGC1α. Mice were fed with a

HFD for 3 weeks, followed by UTMD-assisted exosome delivery. The exosome delivery was performed once a week for 3 continuous weeks (Figure 7A). As shown in Figure 7B, delivery of miR-148a-IRES-PGC1α and delivery of Cap-PGC1α produced significant browning effects, although the extent showed no significant differences. Consistent with the H&E staining results, the body weight displayed a significant decrease in mice delivered with miR-148a-IRES-PGC1α- or Cap-PGC1α-loaded exosomes (Figure 7C), while the food intake had no significant differences (Figure 7D). Moreover, the expression of *Ucp1* and *Cidea* (two known important markers for brown fat) were also increased to a similar level in the adipose tissue of mice delivered with miR-148a-IRES-PGC1α- or Cap-PGC1α-loaded exosomes (Figures 7E and 7F). UCP1 immunostaining further confirmed the above findings (Figure S8). Taken together, these data revealed that delivery of miR-148a-IRES-PGC1α mRNA-loaded exosomes in the adipose tissue produced obvious browning effects with the expected low off-target effects (Figure 7G).

DISCUSSION

To minimize off-target effects, in this study, we developed a novel drug delivery strategy. The main findings of the study include the following: (1) a tissue-specific miRNA translationally activates IRES-modified mRNA when the upstream of the IRES is engineered to be responsive to the miRNA; (2) the engineered mRNA could be

Figure 4. UTMD Assisted Adipose Delivery of Exosomes

(A) Schematic illustration of the experimental procedure. Exosomes were labeled with DiR or DiI and then mixed with ultrasound microbubbles. Adipose delivery of exosomes was assisted by UTMD conducted in the abdominal region. (B) *Ex vivo* imaging of distribution of DiR-labeled exosomes in the adipose tissue with or without UTMD assistance data are expressed as mean ± SEM of three independent experiments. *p < 0.05 versus no UTMD. (C) Confocal microscopy analysis of distribution of DiI-labeled exosomes in the adipose tissue. Representative images of the data of three mice in each group are shown. (D) Schematic illustration of the experimental procedure. Exosomes were encapsulated with *cel*-miR-39, and then the exosomes were mixed with ultrasound microbubbles. Adipose delivery of exosomes was assisted by UTMD conducted in the abdominal region. (E) qPCR analysis of *cel*-miR-39 expression in heart, adipose tissue, lung, spleen, liver, colon, and kidney after exosome delivery *in vivo* with or without UTMD assistance. Data are expressed as mean ± SEM of the results of three mice in each group. *p < 0.05 versus no UTMD.

efficiently encapsulated into functional exosomes and thus able to be translated in the recipient cells; and (3) exosomes encapsulated with miR-148a (an adipose relatively specific miRNA)-responsive PGC1α mRNA could efficiently and specifically activate fat browning when delivered with the aid of UTMD.

Obesity has become a world-wide health burden, which raises the risk for metabolic diseases, cardiovascular diseases, and even cancer.[12] Great advances in understanding the molecular basis of obesity and obesity-associated diseases have been achieved in the past 10 years, making gene therapy a candidate approach for coping with this world-wide problem.[13] Gene therapies for obesity that aim to promote lipolysis and energy expenditure, and to induce fat browning, have been attracting much attention.[14] Among the candidates, PGC1α has been considered as the most appealing one, due to its great role in promoting mitochondria biogenesis and co-activating PRDM16, an essential transcription factor for brown fat induction and maintenance.[15] Efficient and specific delivery of PGC1α in white adipose tissue would be a promising strategy to cope with obesity. With the strategy referred to above, we revealed that PGC1α could be topically delivered and thus safely reduce the fat weight in the targeted region.

Efficient and targeted delivery of nucleic acids is a prerequisite for gene therapy.[16–18] Canonical drug carriers, such as viruses, liposomes, and ultrasound microbubbles, have been extensively studied.[19,20] Taking viruses as an example, genes of interest could be cloned into a virus and thus become functional when the virus infects the target cells. In the virus system, the virus could be tuned to increase the target specificity, and the tissue-specific promoter could be used to additionally avoid the off-target effects.[21] However, the potential carcinogenic risk of virus vectors has limited their clinical applications.[22] Natural exosomes from many tissues or cells have been confirmed to be candidate therapeutic vehicles for many different diseases.[23] Exosomes could cross the blood-brain barrier and maternal-placental barrier, making it a rational vehicle for different diseases.[24,25] Moreover, exosomes could be also manipulated by surface functionalization to improve targeting specificity. However, such engineering is time-consuming. Our present study revealed that the clinically available diagnostic microbubble SonoVue significantly increased the endocytosis of exosomes in the adipose tissues, which means that smaller amounts of exosomes are needed. The strategy is ready for use for all tissues, only if the ultrasound beam could be achieved. As to the mechanism for why UTMD facilitates exosome delivery in refractory tissues, we prefer the model that the microbubble destruction resultant cavitation effect is able to enhance cell membrane permeability, which in turn not only slows the local blood flow, but also activates the uptake activity and efficiency of recipient cells. In any event, the proposed strategy should have broad potential for use in the clinic. Notably, there are no clinical applications of exosomes reported at this time. With the advance of exosomes in gene therapy, the ultrasound-assisted delivery strategy would be right on the shelf to serve as an alternative to improve the targeted delivery and thus reduce the off-target effects via minimizing the dose used.
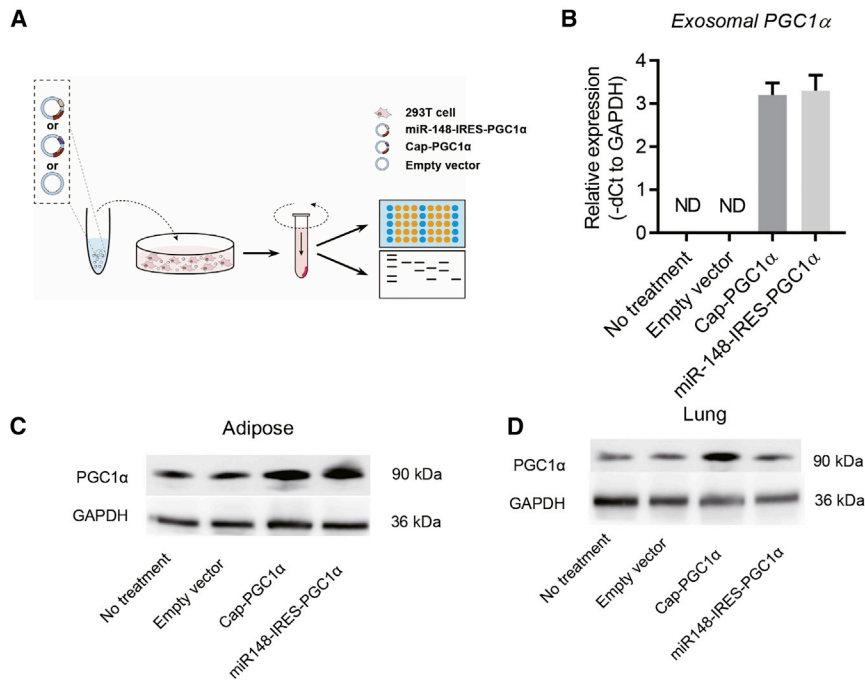
Figure 5. Construction of Adipose-Specific Translation System for PGC1α mRNA

(A and B) qPCR analysis of miR-148a expression in different tissues of chow diet (A) and high-fat diet (B) mice. Data are expressed as mean ± SEM of three biological replicates. (C) Schematic cartoon of the PGC1α expression system whose translation is driven by the miR-148a-IRES. (D) Western blot analysis of PGC1α in B16 cells with indicated treatments. GAPDH served as internal control. Representative image of three biological replicates are shown.

For tissue-responsive delivery, promoter-specific gene delivery is a choice, while the delivered cargo should be DNA and thus should be delivered into the nuclei.[26] The delivered DNA is immunogenic in cytoplasm before its entry into the nuclei. We here for the first time have established a miRNA-responsive IRES system. IRES has been found to be essential for virus replication. Intensive studies have been performed to inhibit viral replication via targeting IRES activity.[27–29] Similarly, IRES-dependent translation has also been found to be important for the expression of some oncogenes, such as myc, and epidermal growth factor receptor during the development of tumors.[30–32] Some pioneering studies have developed a novel strategy to selectively suppressing IRES-driven oncogenic or other pathogenic gene translation based on delivery of disease-specific miRNAs.[33] In contrast, in this study, we developed an IRES-dependent targeted gene expression system by combinatorial use of the tissue-specific miRNA expression pattern. Together with the exosome delivery system, the novel strategy should significantly minimize the off-target effects of gene therapy.

In conclusion, our study for the first time revealed that targeted delivery of exosomes aided by UTMD together with the miRNA-IRES-dependent tissue-specific expression system would induce gene expression in targeted tissues while greatly minimizing the off-target effects in non-targeted tissues, which is of great clinical potential. As a proof-of-concept study, we also found that specifically and efficiently activating PGC1α translation in the adipose tissue is a potent strategy to induce fat browning and holds promise for obesity therapy.

MATERIALS AND METHODS
Animal Housing
Male C57BL/6 mice (8–10 weeks old, 20–22 g) were purchased from the Experimental Animal Center of the Fourth Military Medical University. Mice were maintained under specific pathogen-free conditions with a 12-h light/12-h dark cycle and the temperature kept between 22°C and 24°C. For obesity induction, 6- to 8-week-old male mice were fed with a 45% HFD. All experimental procedures were performed in accordance with guidelines and protocols approved by the Institutional Animal Experiment Administration Committee.

Cell Culture
HEK293T and B16 cells were purchased from ATCC and cultured in DMEM medium (HyClone, Logan, UT, USA) with 10% fetal bovine serum (FBS) and 1% penicillin/streptomycin (HyClone). The cells were maintained in a humidified incubator with 5% CO_2 at 37°C, with the medium changed every 2 days and passaged at the confluence of 90%.

Plasmid Construction
Plasmids expressing GFP, firefly luciferase, and Pgc1α engineered with modified IRES responsive to selected miRNAs were constructed as follows. First, the modified IRES sequences with miRNA recognition sites and flanking cloning sites were designed and synthesized in GenScript, followed by cloning into pcDNA3.1. Then, the CDS regions of GFP, firefly luciferase, and Pgc1α were amplified by PCR with primers harboring restriction enzyme sites EcoRV and BamH1. Then, the amplicons were cloned into the IRES containing pcDNA3.1 plasmid. The right clones were further confirmed by sequencing. The detailed primers and sequences are listed in Tables S1 and S2.

Fluorescence Microscopy
For fluorescence microscopy analysis of tissues, OCT compound-embedded tissues were cut into 8-μm slides and fixed in 4% paraformaldehyde for 20 min at room temperature. After a PBS wash, the slides were incubated with 1 μg/mL Hoechst 33258 for 15 min to counterstain the nuclei. Fluorescence analysis was performed with a confocal laser scanning microscope (Eclipse Ti, Nikon, Tokyo, Japan). For fluorescence microscopy analysis of cells, cultured cells were fixed with 4% paraformaldehyde for 20 min at room temperature, followed by the similar procedure as used for the tissues.

Western Blot
Exosomes, cells, or tissues after indicated treatments were harvested and subjected to radioimmunoprecipitation assay (RIPA) lysis buffer

A

Legend:
- 293T cell
- miR-148-IRES-PGC1α
- Cap-PGC1α
- Empty vector

B

Exosomal PGC1α

Relative expression (-dCt to GAPDH)

ND ND

No treatment / Empty vector / Cap-PGC1α / miR-148-IRES-PGC1α

Figure 6. Adipose-Specific Translation of Delivered miR-148a-IRES-PGC1α mRNA *In Vivo*

(A) Schematic illustration of the experimental procedure. HEK293T cells were transfected with empty vector, routine PGC1α expression vector, or miR-148a-IRES-PGC1α expression vector, followed by exosome isolation and analysis. (B) qPCR analysis of the PGC1α mRNA in the isolated exosomes. Data are expressed as mean ± SEM of three biological replicates. (C and D) Western blot analysis of the PGC1α expression in the adipose tissue (C) and lung (D). GAPDH served as internal control. Data presented are representative of experiments of three mice in each group.

C

Adipose

PGC1α — 90 kDa
GAPDH — 36 kDa

No treatment / Empty vector / Cap-PGC1α / miR148-IRES-PGC1α

D

Lung

PGC1α — 90 kDa
GAPDH — 36 kDa

No treatment / Empty vector / Cap-PGC1α / miR148-IRES-PGC1α

(Beyotime Biotechnology, China) supplemented with protease inhibitor cocktail (Roche). Purified protein was separated in 12% SDS-PAGE (120 V for stacking gel and 160 V for separation gel) and then transferred to a nitrocellulose membrane with an ice bath. The nitrocellulose membrane was blocked with 5% bovine serum albumin for 1 h and then incubated overnight with primary antibodies at 4°C. Antibodies used were mouse anti-GM130, rabbit anti-CD9, rabbit anti-TSG101, rabbit anti-PGC1α, and rabbit anti-GAPDH (all from Abcam). The membrane was then incubated for 1 h with the corresponding secondary antibodies at room temperature and visualized using the enhanced chemiluminescence (ECL) Prime western blotting detection reagent (GE Healthcare, Buckinghamshire, UK).

H&E Staining

The mice were intraperitoneally anesthetized with 120 mg/kg body weight ketamine and 24 mg/kg body weight xylazine in a vehicle containing 0.9% sodium chloride. After complete anesthesia, the mouse thorax was opened and perfused with 4% paraformaldehyde from the apex of the mouse. After perfusion, the adipose tissue was removed and soaked in 4% paraformaldehyde for 24 h. The tissues were placed in the embedding box and rinsed with running water for 30 min. After serial processing, including dehydration, transparency, waxing, embedding, and sectioning, the slides were subjected to H&E staining. Images were observed under a light microscope (Nikon).

qPCR

Total RNA was extracted from the isolated tissues, cells, or exosomes after indicated treatments by TRIzol reagent (Invitrogen, Carlsbad,

CA, USA) according to the manufacturer's instructions. Then, the RNA was reverse transcribed to cDNA using a PrimeScript first-strand cDNA synthesis kit (Takara, Dalian, China), and the relative gene expression at the mRNA level was analyzed using PrimeScript RT master mix (Roche, Switzerland). All PCR reactions were run at least in triplicate, and target mRNA expression was normalized to GAPDH. Relative expression was calculated by normalizing to the control samples using the $2^{-\Delta\Delta Ct}$ method. Absolute quantification PCR analysis of the mRNA copies encapsulated in the exosomes was done as described previously.[34]

Cell Transfection

For cell transfection, HEK293T cells or B16 cells seeded in six-well plates were pretreated with serum-free medium for 6 h and then transfected with 4 μg of plasmid and/or 100 nM miRNAs (detailed sequences in Table S3) using Lipofectamine 2000 (Invitrogen, Carlsbad, CA, USA) according to the manufacturer's protocol. The medium was changed to culture medium 6 h later and cells were additionally incubated at 37°C, 5% CO_2 for either gene expression analysis or in serum-free medium for exosome isolation.

Luciferase Reporter Assay

HEK293T cells seeded in 24-well plates were pretreated with serum-free medium for 6 h and then transfected with 100 nM NC/miRNA mimics, 100 ng of corresponding IRES-Luc reporter plasmid, and 10 ng of internal control pRL-TK (Renilla luciferase driven by the herpes simplex virus [HSV]-thymidine kinase promoter) using Lipofectamine 2000 (Invitrogen, Carlsbad, CA, USA) according to the manufacturer's protocol. The medium was changed to culture medium 6 h later and cells were harvested 24 h later and subjected to passive lysis buffer as instructed. The relative luciferase activity assay was done as described.[35]

Exosome Isolation

HEK293T cells were used as the exosome donor cells in the study. Briefly, the complete growth medium was changed with serum-free
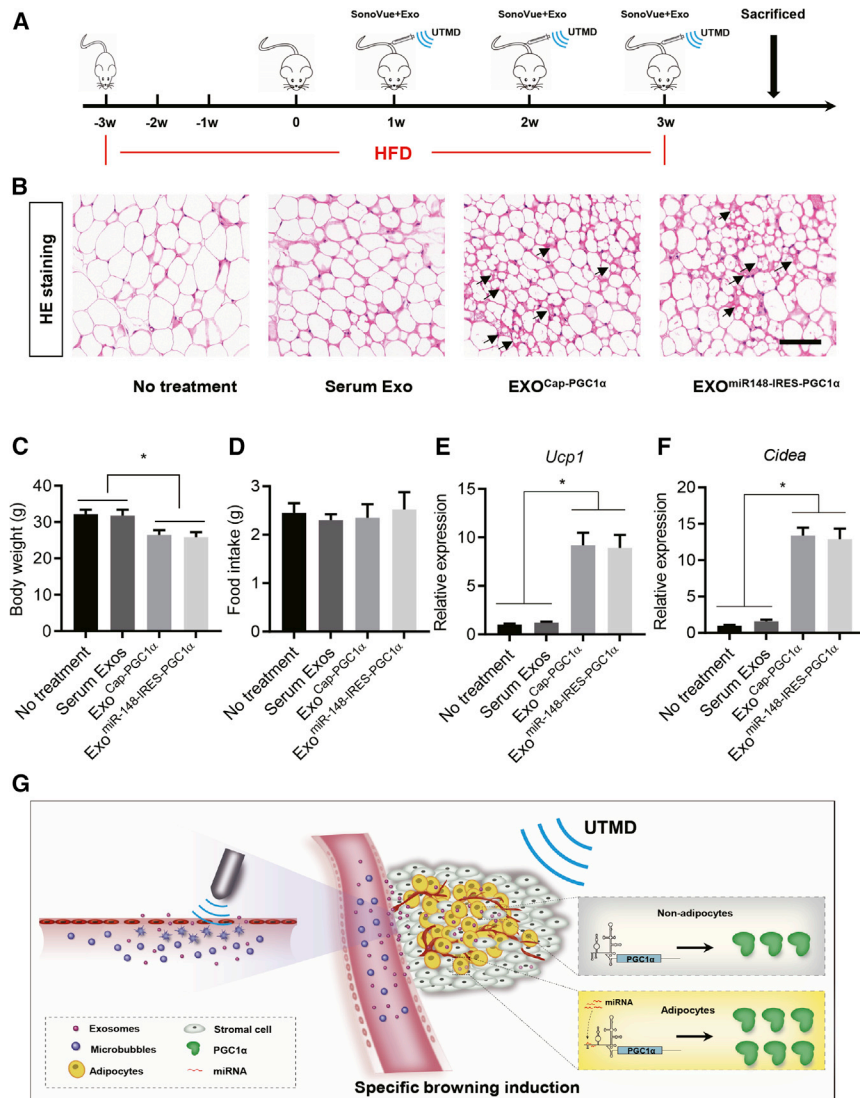
Figure 7. Delivery of mIRES-PGC1α mRNA Efficiently Promotes Browning in High-Fat Diet Mice

(A) Schematic illustration of the experimental procedure. Mice were fed with a high-fat diet for 3 weeks, followed by exosome delivery with the aid of UTMD. The exosome delivery was performed once a week for 3 continuous weeks. Mice were sacrificed at the end of experiments for histology and gene expression. (B) H&E staining of the adipose tissue in mice treated as indicated. Smaller browning adipocytes are indicated by arrows. Scale bar, 50 μm. Data shown are representative of five to seven mice in each group. (C) Body weight in mice treated as indicated. Data are expressed as mean ± SEM of seven mice in each group. *p < 0.05 by one-way ANOVA. (D) Food intake in mice treated as indicated. Data are expressed as mean ± SEM of seven mice in each group. *p < 0.05 by one-way ANOVA. (E and F) qPCR analysis of Ucp1 (E) and Cidea (F) expression in adipose tissue. Gapdh served as internal control. Data are expressed as mean ± SEM of three mice in each group. *p < 0.05 by one-way ANOVA. (G) Schematic illustration of the study.

isoflurane, and the mixture composed of 100 μL of SonoVue microbubble (Bracco Imaging) solution and 100 μL of exosomes was infused into the tail vein slowly. Simultaneously, an ultrasound beam was performed in the targeted organ regions. Ultrasound was generated by a 0.66-MHz US instrument (gift from Chongqing Medical University) with a probe area of 4.5 cm². The probe was adjusted with a gel interface so that the focus was positioned at the targeted tissues. Ultrasound pulses were applied to the targeted region for 1 min in total at a duty cycle of 50% and a mechanical index of about 1.6.

Exosome Tracking In Vivo and Ex Vivo

For in vivo tracking exosomes, purified exosomes were first labeled with fluorescent dye DiR/DiI (at the final concentration of 10 μM, Invitrogen, Carlsbad, CA, USA). Unlabeled free exosomes were then removed by centrifugation after washing with PBS. Mice were then additionally injected with labeled exosomes (100 μg per mouse, at 100 μL in volume) via tail vein with or without the aid of UTMD.

For ex vivo imaging, mice were sacrificed at the end of the experiment. Different tissues from the mice injected with DiR-labeled exosomes were harvested for fluorescence imaging by the IVIS Lumina II in vivo imaging system as instructed. For microscopic analysis of the exosome distribution, different tissues from the mice injected with DiI-labeled exosomes were harvested for tissue sectioning. Tissue sections were fixed with 4% paraformaldehyde for 15 min and then stained with Hoechst 33258 (Invitrogen). The whole process was kept from light. The fluorescence signals for the labeled exosomes and the blue nuclei were visualized by CLSM.

medium when the cell density reached 70% confluence. For the isolation of exosomes, the culture medium was centrifuged at 500 × g for 10 min to remove cells and then at 10,000 × g for 20 min to eliminate the cell debris. Then, the supernatants were filtered through 0.45-μm filters, followed by exosome isolation with an ExoQuick-TC kit. Isolated exosomes from different sources were diluted to 500 ng/mL and subjected to size distribution analysis by NanoSight. The exosome morphology was confirmed by electron microscopy. Briefly, the exosomes were added onto the grid and stained with 2% uranyl acetate, followed by imaging with a JEM-2000EX transmission electron microscope (JEOL, Tokyo, Japan). Isolated exosomes were re-suspended in PBS or DMEM and stored at −80°C use.

Exosome Delivery In Vivo and UTMD

Exosome in vivo delivery aided by UTMD was conducted similar to methods described before.[9] Briefly, mice were anaesthetized with 2%

Statistical Analysis

Data are expressed as mean ± SEM unless otherwise indicated. A Student's t test was used for two-group comparison, and one-way ANOVA was used for multiple comparisons by a Tukey's *post hoc* test (GraphPad Prism 7.0). p values <0.05 indicate statistical significance.

SUPPLEMENTAL INFORMATION

Supplemental Information can be found online at https://doi.org/10.1016/j.omtn.2020.03.016.

AUTHOR CONTRIBUTIONS

W.S. and C.X. performed most of the experiments and drafted the manuscript. L.Z. performed some of the experiments and analyzed the data. P.Z. assisted in the animal experiment. G.Y. and L.Y. designed experiments. All authors read and approved the final manuscript.

CONFLICTS OF INTEREST

The authors declare no competing interests.

REFERENCES

1. Contreras-Naranjo, J.C., Wu, H.J., and Ugaz, V.M. (2017). Microfluidics for exosome isolation and analysis: enabling liquid biopsy for personalized medicine. Lab Chip *17*, 3558–3577.

2. Barile, L., and Vassalli, G. (2017). Exosomes: therapy delivery tools and biomarkers of diseases. Pharmacol. Ther. *174*, 63–78.

3. Alvarez-Erviti, L., Seow, Y., Yin, H., Betts, C., Lakhal, S., and Wood, M.J. (2011). Delivery of siRNA to the mouse brain by systemic injection of targeted exosomes. Nat. Biotechnol. *29*, 341–345.

4. El Andaloussi, S., Lakhal, S., Mäger, I., and Wood, M.J. (2013). Exosomes for targeted siRNA delivery across biological barriers. Adv. Drug Deliv. Rev. *65*, 391–397.

5. Jüttner, J., Szabo, A., Gross-Scherf, B., Morikawa, R.K., Rompani, S.B., Hantz, P., Szikra, T., Esposti, F., Cowan, C.S., Bharioke, A., et al. (2019). Targeting neuronal and glial cell types with synthetic promoter AAVs in mice, non-human primates and humans. Nat. Neurosci. *22*, 1345–1356.

6. Schult, P., Roth, H., Adams, R.L., Mas, C., Imbert, L., Orlik, C., Ruggieri, A., Pyle, A.M., and Lohmann, V. (2018). microRNA-122 amplifies hepatitis C virus translation by shaping the structure of the internal ribosomal entry site. Nat. Commun. *9*, 2613.

7. Landgraf, P., Rusu, M., Sheridan, R., Sewer, A., Iovino, N., Aravin, A., Pfeffer, S., Rice, A., Kamphorst, A.O., Landthaler, M., et al. (2007). A mammalian microRNA expression atlas based on small RNA library sequencing. Cell *129*, 1401–1414.

8. Henke, J.I., Goergen, D., Zheng, J., Song, Y., Schüttler, C.G., Fehr, C., Jünemann, C., and Niepmann, M. (2008). microRNA-122 stimulates translation of hepatitis C virus RNA. EMBO J. *27*, 3300–3310.

9. Sun, W., Li, Z., Zhou, X., Yang, G., and Yuan, L. (2019). Efficient exosome delivery in refractory tissues assisted by ultrasound-targeted microbubble destruction. Drug Deliv. *26*, 45–50.

10. Shi, C., Zhang, M., Tong, M., Yang, L., Pang, L., Chen, L., Xu, G., Chi, X., Hong, Q., Ni, Y., et al. (2015). miR-148a is associated with obesity and modulates adipocyte differentiation of mesenchymal stem cells through Wnt signaling. Sci. Rep. *5*, 9930.

11. Pan, D., Fujimoto, M., Lopes, A., and Wang, Y.X. (2009). Twist-1 is a PPARδ-inducible, negative-feedback regulator of PGC-1α in brown fat metabolism. Cell *137*, 73–86.

12. Saltiel, A.R., and Olefsky, J.M. (2017). Inflammatory mechanisms linking obesity and metabolic disease. J. Clin. Invest. *127*, 1–4.

13. Jimenez, V., Jambrina, C., Casana, E., Sacristan, V., Muñoz, S., Darriba, S., Rodó, J., Mallol, C., Garcia, M., León, X., et al. (2018). FGF21 gene therapy as treatment for obesity and insulin resistance. EMBO Mol. Med. *10*, e8791.

14. Dempersmier, J., Sambeat, A., Gulyaeva, O., Paul, S.M., Hudak, C.S., Raposo, H.F., Kwan, H.Y., Kang, C., Wong, R.H., and Sul, H.S. (2015). Cold-inducible Zfp516 activates UCP1 transcription to promote browning of white fat and development of brown fat. Mol. Cell *57*, 235–246.

15. Boström, P., Wu, J., Jedrychowski, M.P., Korde, A., Ye, L., Lo, J.C., Rasbach, K.A., Boström, E.A., Choi, J.H., Long, J.Z., et al. (2012). A PGC1-α-dependent myokine that drives brown-fat-like development of white fat and thermogenesis. Nature *481*, 463–468.

16. Rupaimoole, R., and Slack, F.J. (2017). MicroRNA therapeutics: towards a new era for the management of cancer and other diseases. Nat. Rev. Drug Discov. *16*, 203–222.

17. Rosenblum, D., Joshi, N., Tao, W., Karp, J.M., and Peer, D. (2018). Progress and challenges towards targeted delivery of cancer therapeutics. Nat. Commun. *9*, 1410.

18. Naldini, L. (2015). Gene therapy returns to centre stage. Nature *526*, 351–360.

19. Sawant, R.R., and Torchilin, V.P. (2012). Challenges in development of targeted liposomal therapeutics. AAPS J. *14*, 303–315.

20. Karimi, M., Mirshekari, H., Moosavi Basri, S.M., Bahrami, S., Moghoofei, M., and Hamblin, M.R. (2016). Bacteriophages and phage-inspired nanocarriers for targeted delivery of therapeutic cargos. Adv. Drug Deliv. Rev. *106* (Pt A), 45–62.

21. Isgrig, K., McDougald, D.S., Zhu, J., Wang, H.J., Bennett, J., and Chien, W.W. (2019). AAV2.7m8 is a powerful viral vector for inner ear gene therapy. Nat. Commun. *10*, 427.

22. Chen, Y.H., Keiser, M.S., and Davidson, B.L. (2018). Viral vectors for gene transfer. Curr. Protoc. Mouse Biol. *8*, e58.

23. Rodríguez, J.M., Wolfrum, S., Robblee, M., Chen, K.Y., Gilbert, Z.N., Choi, J.H., Teupser, D., and Breslow, J.L. (2013). Altered expression of *Raet1e*, a major histocompatibility complex class 1-like molecule, underlies the atherosclerosis modifier locus *Ath11* 10b. Circ. Res. *113*, 1054–1064.

24. Nair, S., and Salomon, C. (2018). Extracellular vesicles and their immunomodulatory functions in pregnancy. Semin. Immunopathol. *40*, 425–437.

25. Rufino-Ramos, D., Albuquerque, P.R., Carmona, V., Perfeito, R., Nobre, R.J., and Pereira de Almeida, L. (2017). Extracellular vesicles: novel promising delivery systems for therapy of brain diseases. J. Control. Release *262*, 247–258.

26. Zheng, C., and Baum, B.J. (2008). Evaluation of promoters for use in tissue-specific gene delivery. Methods Mol. Biol. *434*, 205–219.

27. Dasgupta, A., Das, S., Izumi, R., Venkatesan, A., and Barat, B. (2004). Targeting internal ribosome entry site (IRES)-mediated translation to block hepatitis C and other RNA viruses. FEMS Microbiol. Lett. *234*, 189–199.

28. Gasparian, A.V., Neznanov, N., Jha, S., Galkin, O., Moran, J.J., Gudkov, A.V., Gurova, K.V., and Komar, A.A. (2010). Inhibition of encephalomyocarditis virus and poliovirus replication by quinacrine: implications for the design and discovery of novel antiviral drugs. J. Virol. *84*, 9390–9397.

29. Davis, D.R., and Seth, P.P. (2011). Therapeutic targeting of HCV internal ribosomal entry site RNA. Antivir. Chem. Chemother. *21*, 117–128.

30. Stoneley, M., Subkhankulova, T., Le Quesne, J.P., Coldwell, M.J., Jopling, C.L., Belsham, G.J., and Willis, A.E. (2000). Analysis of the c-*myc* IRES; a potential role for cell-type specific trans-acting factors and the nuclear compartment. Nucleic Acids Res. *28*, 687–694.

31. Jopling, C.L., Spriggs, K.A., Mitchell, S.A., Stoneley, M., and Willis, A.E. (2004). L-Myc protein synthesis is initiated by internal ribosome entry. RNA *10*, 287–298.

32. Webb, T.E., Hughes, A., Smalley, D.S., and Spriggs, K.A. (2015). An internal ribosome entry site in the 5′ untranslated region of epidermal growth factor receptor allows hypoxic expression. Oncogenesis *4*, e134.

33. Miyazaki, Y., Du, X., Muramatsu, S., and Gomez, C.M. (2016). An miRNA-mediated therapy for SCA6 blocks IRES-driven translation of the *CACNA1A* second cistron. Sci. Transl. Med. *8*, 347ra94.

34. Li, Z., Zhou, X., Wei, M., Gao, X., Zhao, L., Shi, R., Sun, W., Duan, Y., Yang, G., and Yuan, L. (2019). In vitro and in vivo RNA inhibition by CD9-HuR functionalized exosomes encapsulated with miRNA or CRISPR/dCas9. Nano Lett. *19*, 19–28.

35. Yang, G., Yu, F., Fu, H., Lu, F., Huang, B., Bai, L., Zhao, Z., Yao, L., and Lu, Z. (2007). Identification of the distinct promoters for the two transcripts of apoptosis related protein 3 and their transcriptional regulation by NFAT and NFκB. Mol. Cell. Biochem. *302*, 187–194.